# Structural mechanism of the interaction of Alzheimer's disease $A\beta$ fibrils with the NSAID sulindac sulfide

Elke Prade,<sup>†</sup> Heiko J. Bittner,<sup>‡</sup> Riddhiman Sarkar, <sup>†</sup> Juan Miguel Lopez del Amo, <sup>§</sup> Gerhard Althoff-Ospelt,<sup>‡</sup> Gerd Multhaup, <sup>¶</sup> Peter W. Hildebrand, <sup>‡</sup> Bernd Reif<sup>o,†,</sup><sub>v</sub>

\* Running title: NSAIDs interact specifically with Amyloid-β fibrils

**KEYWORDS:** Alzheimer's disease · solid-state NMR · drug design · amyloid · protein drug interactions

**Background**: The mechanism of interaction between small molecules and amyloid- $\beta$  fibrils is unknown.

**Results**: Molecular modeling based on solid-state NMR reveals that sulindac sulfide intercalates between  $\beta$ -strands of amyloid- $\beta$  fibrils.

**Conclusion:** Sulindac sulfide interacts with amyloid- $\beta$  fibrils in a specific manner and may alter M35 oxidation.

**Significance**: Unraveling how small molecules interfere with amyloidogenic deposits will assist structure-based drug design for neurodegenerative disorders.

**ABSTRACT:** Alzheimer's disease is the most severe neurodegenerative disease worldwide. In the past years, a plethora of small molecules interfering with amyloid- $\beta$  (A $\beta$ ) aggregation have been suggested. However, their mode of interaction with amyloid fibers is not understood. Non-steroidal anti-inflammatory drugs (NSAIDs) are known  $\gamma$ -secretase modulators (GSMs). It has been suggested that NSAIDs are pleiotrophic and can interact with more than one pathomechanism. We present here a magic angle spinning (MAS) solid-state NMR study that shows that the NSAID sulindac sulfide interacts specifically with Alzheimer's disease A $\beta$  fibrils. We find that

sulindac sulfide does not induce drastic architectural changes in the fibrillar structure, but intercalates between the two  $\beta$ -strands of the amyloid fibril and binds to hydrophobic cavities, which are found consistently in all analyzed structures. The characteristic D23-K28 salt bridge is not affected upon interacting with sulindac sulfide. The primary binding site is located in the vicinity of residue G33, a residue involved in M35 oxidation. The results presented here could be useful in the search for pharmacologically active molecules which can potentially be employed as lead structures to guide the design of small molecules for the treatment of Alzheimer's disease.

#### INTRODUCTION

The self-assembly of amyloidogenic proteins into fibrils and oligomers plays a pivotal role in various diseases (1). The deposition of fibrils formed by the amyloid- $\beta$  peptide (A $\beta$ ) into plaques in brain tissue is a major pathological hallmark in the progression of neurodegeneration in Alzheimer's disease (AD). A $\beta$  peptides are generated through sequential proteolytic cleavages of the amyloid precursor protein (APP) by the  $\beta$ -and  $\gamma$ -secretases (2,3). This results in the

<sup>&</sup>lt;sup>†</sup> Munich Center for Integrated Protein Science (CIPS-M) at Department Chemie, Technische Universität München (TUM), Lichtenbergstr. 4, 85747 Garching, Germany.

<sup>&</sup>lt;sup>‡</sup> Molecular Modeling, Institute of Medical Physics and Biophysics, Universitätsmedizin Berlin, Charitéplatz 1, Berlin, Germany.

<sup>§</sup> Current address: CIC Energigune, Albert Einstein 48, 01510 Miñano, (Álava), Spain.

<sup>&</sup>lt;sup>1</sup> Bruker BioSpin, Silberstreifen 4, 76287 Rheinstetten, Germany.

Department of Pharmacology & Therapeutics, McGill University, 3655 Promenade Sir-William-Osler, Montreal QC, H3G 1Y6, Canada.

<sup>&</sup>lt;sup>▽</sup> Helmholtz-Zentrum München (HMGU), Deutsches Forschungszentrum für Gesundheit und Umwelt, Ingolstädter Landtstr. 1, 85764 Neuherberg, Germany.

<sup>°</sup> Corresponding author: Bernd Reif, email: reif@tum.de

production of AB peptides of differing lengths (4), mainly  $A\beta_{1-40}$  and  $A\beta_{1-42}$  (5), and shorter variants such as  $A\beta_{1-39}$  (6). Soluble oligomers formed by  $A\beta_{1-42}$  represent the toxic species responsible for decline in cognitive function associated with neurodegeneration (7). Several studies have demonstrated that small molecules can interfere with the solubility of amyloid proteins and are therefore potential drug candidates (8,9). Chronic inflammation enhances significantly pathogenesis (10). Fibrillar β-amyloid deposits colocalize with numerous chronic inflammatory mediators and activated microglia in the brain (11). The relation to inflammation suggests that non-steroidal anti-inflammatory drugs (NSAIDs) might be beneficial for the treatment of AD. In fact, epidemiological studies demonstrate a link between the use of anti-inflammatory drugs and prevalence of AD (12). The presented work aims to investigate the interaction mechanism of the NSAID sulindac sulfide (Figure 1a) with the Alzheimer's peptide Aß fibrils. In addition to sulindac sulfide (13),**NSAIDs** including ibuprofen, indomethacin (13), and flurbiprofen been identified (14) have as γ-secretase modulators (GSMs). GSMs interfere with APP modify the relative  $A\beta_{1-42}$ processing and population. In particular, sulindac sulfide decreases relative amount the of the amyloid-prone  $A\beta_{1-42}$ , while the production of shorter, less amyloidogenic Aß peptides is increased (13-16).

Solution-state NMR structures of the APP-TM (transmembrane) dimer have been solved for the wild-type (17) and a familial mutant (18). NMR and EPR experiments revealed a potential cholesterol-binding site within the C-terminal C99 sequence and highlight the significance of the GxxxG segments for binding (19). It has been suggested that NSAIDs can interact with lipids to form phospholipid complexes (20-22). This may provide a general mechanism for the interaction of APP with small molecules. Reports on the interaction between sulindac sulfide and APPtransmembrane sequence (APP-TMS) are however contradictory. Sulindac sulfide, among other GSMs, binds to the APP-TMS of the C99 motif (23), and to C100 dimers in the presence of SDS micelles (24). Bacterial reporter assays show that GSMs including sulindac sulfide bind to the

GxxxG dimerization motif and thereby attenuate dimerization of the APP-TMS (25), a process necessary for proteolytic cleavage (26). However, colloidal aggregation of sulindac sulfide in aqueous solutions can potentially induce nonspecific binding (27,28). Contradicting data has been reported for the influence of sulindac sulfide on the A $\beta$  peptide itself (29,30).

So far, it is not understood how sulindac sulfide interacts with amyloids. NMR is a suitable technique to study Aß-ligand interactions for various Aß aggregation states (31). Solution-state NMR can be employed to study interactions of Aβ monomers and small molecule (32) or peptide inhibitors (33), nanoparticles (34) and various others. Besides monomers and fibrils, oligomeric intermediates formed by AB in solution constitute (35,36).potential drug targets However. oligomeric intermediates and insoluble fibrils are not detectable by solution-state NMR as their lines are broadened beyond detection. Solid-state NMR spectroscopy is a powerful tool that allows studying Aβ-small molecule interactions at atomic resolution. In the past, this technique has been successfully applied for the characterization of the interaction between AB and the polyphenol epigallocatechin gallate (37), curcumin (38,39) and catechol-type flavonoids (40), as well as to study the interface of congo red and amyloids formed by the prion domain of the HET-s protein (41). In the work presented here, we investigate the interaction between sulindac sulfide and AB fibrils using solid-state NMR spectroscopy. On the basis of the gathered NMR data, we employ flexible docking to derive a model for the intercalation of sulindac sulfide with Aß fibrils.

#### **EXPERIMENTAL PROCEDURES**

## $\boldsymbol{A}\boldsymbol{\beta}$ expression and purification and sample preparation

The uniformly  $^{15}$ N, or  $^{15}$ N- $^{13}$ C labeled A $\beta_{1-40}$  peptide was recombinantly expressed in *E.coli* inclusion bodies and purified via reverse-phase chromatography as previously described (42). The construct contains an N-terminal methionine, but shows the same biochemical properties as the wildtype peptide (43). To obtain monomeric A $\beta$  in solution, the lyophilized peptide was initially

dissolved in 10 mM NaOH, sonicated for 10 min in an ultrasonic bath, and centrifuged for 10 min at 14800 RPM to remove potential nucleation seeds. The solution was then diluted in 2X buffer (100 mM sodium phosphate + 100 mM NaCl buffer pH 7.3) to yield the respective  $A\beta$  concentration.

#### **Preparation of NSAIDs**

Stock solutions of sulindac sulfide were prepared in dimethyl-sulfoxide (DMSO), and the respective amount of NSAID stock was added to  $A\beta$ . The final concentration of DMSO in aqueous solutions was 1%.

#### **Solid-state NMR sample preparation**

Aß fibrils were obtained according to a protocol described previously (44). Briefly, monomeric AB at a concentration of 50 µM was seeded with sonicated fibrils (10% w/w) and incubated under agitation until the completion of fibrillation. This step was repeated for 11 generations. For solid-state NMR measurements, the last generation was allowed to fibrilize for 2 days before sulindac sulfide was added to the sample. Approximately 10 mg of Aβ fibrils were incubated with a 5-fold molar excess of sulindac sulfide (250 µM, 1% DMSO). After mixing, the sample was kept quiescently for 1 h at room temperature. As a reference, AB fibrils were incubated under the same conditions with 1% DMSO. The sulindac sulfide incubated fibrils were sedimented into a 3.2 mm rotor. The reference fibrils were packed into a 4.0 mm rotor.

#### **Solid-state NMR measurements**

<sup>13</sup>C detected assignment experiments were carried out using a Bruker Avance wide bore spectrometer operating at a <sup>1</sup>H Larmor frequency of 700 MHz (16.5 Tesla). The spectrometer was equipped with a triple resonance MAS probe (<sup>1</sup>H, <sup>13</sup>C, <sup>15</sup>N). All measurements were recorded at a MAS rotation frequency of 17 kHz for 3.2 mm rotors, or 13 kHz for 4.0 mm rotors and a temperature of 12 °C. In all experiments, <sup>1</sup>H-<sup>13</sup>C magnetization transfer was achieved through cross polarization (CP). 2D spectra were recorded using proton-driven spin diffusion (PDSD) (45,46) for <sup>13</sup>C-<sup>13</sup>C magnetization transfer, with a mixing time of 200 ms, or transferred echo double resonance (TEDOR) (47,48) for <sup>13</sup>C-<sup>15</sup>N magnetization

transfer. The 3D NCACX and NCOCX (49) experiments were recorded employing TEDOR for <sup>13</sup>C -<sup>15</sup>N magnetization transfer, and dipolar assisted rotational resonance (DARR) (50) for <sup>13</sup>C-<sup>13</sup>C mixing.

To identify <sup>13</sup>C atoms in Aβ which are located in the vicinity of the <sup>19</sup>F atom of sulindac sulfide, we recorded <sup>13</sup>C-<sup>19</sup>F rotational echo double resonance (REDOR) experiments (Figure S8a) (51). These were recorded on a Bruker Avance III wide bore spectrometer operating at a <sup>1</sup>H Larmor frequency of 600 MHz (14 Tesla). spectrometer was equipped with a triple resonance CP MAS probe (<sup>1</sup>H, <sup>13</sup>C, <sup>19</sup>F). All measurements were recorded at a MAS rotation frequency of 14.6 kHz and a temperature of 12 °C. In all measurements <sup>1</sup>H-<sup>13</sup>C ramped CP (on <sup>1</sup>H channel; 75%-100% for <sup>13</sup>C-<sup>13</sup>C PDSD and <sup>13</sup>C-<sup>15</sup>N TEDOR spectra; 90%-100% for <sup>13</sup>C-<sup>19</sup>F REDOR) was employed for the initial magnetization transfer. In the REDOR experiments,  ${}^{13}\text{C}{}^{-19}\text{F}$  dipolar dephasing was preceded by a  ${}^{13}\text{C}{}^{-13}\text{C}$  PDSD mixing step. REDOR dephasing times were set to 1.1 ms, 2.2 ms and 4.4 ms. REDOR spectra recorded with and without dephasing pulses were subtracted to identify fluorine-coupled carbons. In Figure 2a, REDOR spectra are represented in 1D-mode. No <sup>13</sup>C-<sup>13</sup>C cross peaks could be observed in the 3D-REDOR experiments, as the sensitivity was too low. In order to detect the characteristic salt bridge between the carboxyl of D23 and the amine of K28 of mature A\beta fibrils, TEDOR experiments (Figure S8b) were carried out based on the pulse sequence described by Jaroniec et al (52). All spectra were recorded at a Bruker Avance III narrow bore spectrometer operating at a <sup>1</sup>H Larmor frequency of 750 MHz (17.63 Tesla) equipped with a triple resonance MAS probe (<sup>1</sup>H, <sup>13</sup>C, <sup>15</sup>N) at a MAS rotation frequency of 11 kHz and 4 °C. In the experiment, the TEDOR mixing time was set to 7.27 ms and 15.72 ms.

#### Transmission electron microscopy (TEM)

Images were recorded on an EM 900 from Carl Zeiss SMT. Samples were stained with 4% uranyl acetate solution on formvar/carbon coated grids.

#### Molecular modeling

The 2-fold-symmetric (PDB-ID: 2LMN) (53), as well as the 3-fold-symmetric (PDB-ID: 2LMP) (54) Aβ<sub>1-40</sub> fibril NMR structural models were employed in molecular modeling studies. To identify internal cavities, each model of the AB fibril was analyzed separately. For the calculation of internal cavities, van der Waals (vdW) volumes were derived using the Voronoi cell method (55,56). Atomic volumes are calculated based on the allocation of space among atoms using hyperbolic surfaces (applying a cubic lattice of 0.1 Å grid width) and applying the ProtOr (57) atom radius set for protein atoms that were determined analytically from reference structures. Internal cavities are determined analytically from each model structure by a Delaunay triangulation (58). An internal cavity is defined as the buried space within a structure that is big enough to accommodate at least a 1.4 Å radius water-sized probe. The size of a cavity is estimated from the average distance of the cavity center to the neighboring atoms and depicted by the radius of a sphere. The polarity of the cavities is assessed with the program DOWSER (59) that calculates potential positions for water not resolved by the original structure determination approach. This program assesses the hydrophilicity of protein cavities by determining the interaction energy between a water molecule and its surrounding Water molecules with interaction atoms. energies < -10 kcal/mol are considered 'low energy water molecules' and selected for output. Internal cavities harboring such an internal water molecule are denoted as polar (blue), the remaining cavities as hydrophobic (gray) (Figure 3, S4-S5).

For induced fit docking (60,61), the region between the two most hydrophobic cavity clusters near I32 (#2) and V36 (#3) from the first NMR model was targeted. Docking was performed using Schrödingers Maestro suite (62) following a standard protocol. Subsequently, a grid with auto-assigned box size was generated. The resulting box is centered near an interior L34 for the 3-fold-symmetric structure and an interior I32 and V36 for the 2-fold symmetric structure. Induced fit docking was done with the program Glide with single precision and with no constraints applied (63). To simulate receptor flexibility side

chain orientations were optimized to take into account ligand binding. At last, a Glide redocking was applied for the refined structure. Docking poses are ranked and filtered by means of the Glide score. This score assesses the binding probability and accounts for steric clashes, vdW-and coulomb-energy, lipophilicity, H-bonding and bond rotation ability, among others. Only the energetically most favorable docking poses (with energies < 30 kcal/mol higher than the best pose) are considered for further analysis.

#### RESULTS

To probe the interaction between Aβ fibrils and sulindac sulfide (Figure 1a), we titrated sulindac sulfide to preformed fibrils. The resulting <sup>13</sup>C-<sup>15</sup>N (Figure 1c) and <sup>13</sup>C-<sup>13</sup>C (Figure S1) correlation spectra show well-dispersed peaks. The 3D NCACX and NCOCX experiments allowed sequential assignment of resonances for residues Q15-V40 for both samples (representative strip plots are shown in Figure S2, all assigned resonances are listed in Table S2). We detect only one set of resonances for both samples, indicating that the fibrils exist in one conformation.

Sulindac sulfide has no significant effect on the fibrillar structure of Aβ, as the spectra of both samples are relatively similar (Figures 1c, S1). However, small, yet defined CSPs are observed in the presence of sulindac sulfide, indicating specific interactions of the NSAID with the fibrils. This is remarkable, as a non-quantitative and nonspecific binding of sulindac sulfide to AB fibrils would result in peak splitting and line broadening. Figure 1d shows CSPs  $\Delta\delta$  (ppm) upon addition of sulindac sulfide. We observe changes in chemical shift in particular for side chain resonances, in particular K16, V18-Cβ, F19-Cβ, F20-Cβ, N27-Cγ, M35-Cβ, as well as for the backbone resonances of F19, F20, A21 and G33. CSPs reflect ligand binding, but could as well be a consequence of local or global structural rearrangements. In order to unambiguously probe ligand binding, we recorded <sup>13</sup>C-<sup>19</sup>F REDOR experiments employing the NMR-active properties of the <sup>19</sup>F atom of sulindac sulfide. In general, only aliphatic resonances of AB could be detected. For comparison, a 1D-13C spectrum containing assignments for all aliphatic resonances is

represented (Figure 2a). The strongest dephasing effects are observed for the  $C\gamma$  resonances of V18 or V39. However, due to spectral overlap, these two peaks cannot be discriminated. Smaller signal attenuations are observed for  $C\gamma$  of V24 and V36,  $C\beta$ s of A21 or A30 (overlap), as well as for  $C\gamma$ 2 and  $C\delta$ 1 of I32 at longer mixing times. These resonances exhibit the most severe dephasing effects. The respective residues must thus be located close to the fluorine atom of sulindac sulfide.

In order to gain information on potential effects of sulindac sulfide on the A $\beta$  fibril structure, we investigate the impact on the salt bridge, which is typically formed between the side chains of residues D23 and K28 (53,54). From sequential assignments, the chemical shift of the carboxylic group of D23 in the presence of sulindac sulfide was assigned to 177.8 ppm and to 178.0 ppm for the reference fibrils. Based on 1D- $^{15}$ N spectra, the chemical shift of K28-N $\zeta$  was found to be 33.9 ppm and 34.3 ppm for the two preparations, respectively. In both samples, a cross peak between K28-N $\zeta$  and D23-C $\gamma$  was detected, implying the presence of a salt bridge in both cases (Figure 2b).

In the following, the CSPs in the 2D <sup>13</sup>C-<sup>13</sup>C PDSD and <sup>13</sup>C-<sup>15</sup>N TEDOR, as well as the <sup>13</sup>C-<sup>19</sup>F REDOR contacts are used as restraints to derive a molecular docking model for sulindac sulfide in complex with  $A\beta_{1-40}$  fibrils. We use both the 2-fold (53) and 3-fold-symmetric (54)  $A\beta_{1-40}$  fibril NMR structure as reference structures for modeling and docking experiments, as they show the highest correlation to our chemical shifts (Figure S3) compared to all structures and models analyzed (44,53,54,64-68). These NMR structures contain ten models each. The architecture of the  $A\beta_{1-40}$  fibrils obviously differs comparing the 2fold and 3-fold symmetric structures. In each structure, Aβ adopts a β-strand—turn—β-strand fold. Fibrils are stabilized by hydrogen bonds connecting individual β-strands along the fibril The 3-fold-symmetric fibril structure axis. contains three stacks of AB molecules in a triangular form. The 2-fold-symmetric fibril structure is build from two antiparallel stacks of Aβ molecules. To detect potential binding sites for the hydrophobic sulindac sulfide, we performed a packing analysis for each Aß structure. In fact, all

models reveal large packing defects. On average, we find eight cavities per stack of four Aβ molecules in both structures (Figure S4 and S5) clustering in five different regions within one stack. (clusters #1 - #5) (Figure 3). To dissect polar from unpolar cavities we applied the tool DOWSER (59) to calculate positions of internal water molecules that are not resolved in the NMR structures. We find that the most hydrophobic cavities in each structure cluster in the rigid core region with water occupancies of < 10 % in cluster #2 and < 30 % in cluster #3 that are located on both sides of F19 (Table S3). The 3fold-symmetric structure seems to be more tightly packed around cluster #2 and #3 featuring fewer cavities in comparison to the 2-fold-symmetric structure. At the same time, other clusters in the 3-fold-symmetric structure seem to contain a larger numbers of cavities. Clusters of polar cavities are found in the flexible turn region between residues E22 and I31 (cluster #1) and towards the termini of the peptide sequence (cluster #4). The two structures differ in their interface architecture between the termini to the adiacent loop region. While in the 3-fold-symmetric structure cavities of cluster #4 are stabilized through interactions with the loop, in the 2-fold-symmetric structure fewer polar cavities are found, because the structure opens and cavities can become exposed. Cluster #5 (around M35) polar cavities is located at intersheet/contact region between termini and the loop region (3-fold-symmetric structure), or at the interface of the antiparallel β-sheets (2-foldsymmetric structure). In the intersheet region, where the contact interface between 3-fold- and 2-fold-symmetric structure is apparently different, the amount of cavities per stack (of four AB molecules) and their polarity does not differ. The amount of cavities and the respective water contents per cluster #1 - #5 are shown in Table S3.

Clusters #2 and #3 contain large hydrophobic cavities, which could in principle bury a sulindac sulfide molecule. The exact size of the individual cavities depends on the rotameric state of F19. The 3-fold-symmetric and the 2-fold-symmetric structures differ slightly in the position of F19 with respect to the registry of the second  $\beta$ -sheet containing residues I32 to V36 (Figure S6). In the 3-fold-symmetric structure F19 is oriented more

towards I32, whereas in the 2-fold-symmetric structure F19 is pointing towards L34 and is therefore located more central in the core region. Surprisingly, the size, polarity and distribution of the detected cavities is very similar in all analyzed structural models, even though there are slight differences between the two models.

To test whether the hydrophobic cavities in clusters #2 and #3 are indeed suitable binding sites for sulindac sulfide, we applied an induced fit docking approach, where the sulindac sulfide and side chains of Aβ were kept flexible. The size and accessibility of these cavities depends on the rotameric state of F19. In fact, docking into cluster #3 of the 3-fold-symmetric structure allows to identify two scenarios that fit to the distance restraints obtained from the NMR analysis. In particular, we find that the distance of the sulindac sulfide <sup>19</sup>F-atom to the methyl groups of I32, L34 or V36 is smaller than 6 Å. In pose 1, sulindac sulfide lies in the G33 groove and is orientated along the fibril axes, being close to I32 and L34 The aromatic side chains of F19 are directed towards A30 (Figure 4a, top). In pose 2, sulindac sulfide has rotated into a position with its conjugated ring system parallel to the β-sheets and orthogonal to F19, so that the <sup>19</sup>F-atom approaches L34 and V36. (Figure 4a, bottom). Both poses suggest an aromatic  $\pi$ -stacking interaction between the conjugated ring system of sulindac sulfide and the F19 side chain. Similar interactions are obtained from docking to cluster #2 of the 2-fold-symmetric structure (Figure 4b). In pose 1, sulindac sulfide is orientated along the fibril axes. with its conjugated ring system parallel to F19, analogous to pose 1 in the 3-fold-symmetric structure. Again, the <sup>19</sup>F-atom is positioned in the G33 groove close to I32 and L34. In contrast to the 3-fold symmetric structure, F19 is positioned here on the other side of sulindac sulfide close to L34, thereby shielding V36, so that sulindac sulfide cannot change into a position to contact V36 (Figure 4b, top). An additional docking to cluster #3 yields poses 2 and 3, where the normal of the conjugated ring system of sulindac sulfide is orientated perpendicular to the fibril axes. Thereby, sulindac sulfide extends into the terminal region (#4). The conjugated ring system is positioned parallel to the β-sheets and orthogonal to F19. Sulindac sulfide is either orientated in a way that the <sup>19</sup>F-atom faces F19, L34 and V36 (Figure 4b, center), or that the <sup>19</sup>F-atom is oriented towards the fibril exterior contacting V36 and V39 (Figure 4b, bottom).

#### **DISCUSSION**

Sulindac sulfide incubated AB fibrils are highly similar in comparison to control fibrils implying that sulindac sulfide has no significant effect on fibril structure. Both, the NMR chemical shift patterns, as well as the morphology in TEM images (Figure 1b) are maintained. Analysis of <sup>13</sup>C chemical shifts predicts β-strands as the main secondary structural element in both fibril preparations. In addition, chemical shift analysis by torsion angle likeliness obtained from shift and sequence similarities+ (TALOS+) (69) vields secondary structural propensities that predict the presence of two β-strands typically observed in regions within specific  $A\beta_{1-40}$ fibrils (44,53,54,67,70),oligomers (71,72).and Furthermore, we find in our TEDOR experiments that the D23-K28 salt bridge remains intact in the presence of sulindac sulfide (Figure 2b). Even though the overall fibrillar character is maintained, we observe defined chemical shift changes indicating local conformational changes. Previous reports have stated that small molecules such as curcumin (39) are able to disrupt the characteristic salt bridge in  $A\beta_{1-42}$  fibrils. Comparison of the EM data for the two samples suggests that curcumin has a more drastic effect on the general fibril architecture as it disrupts  $A\beta_{1-42}$  fibrils (39). We note that only one set of resonances is observed for the sulindac sulfide incubated Aß fibrils. For none of the cross peaks, a splitting of the resonances is observed. Rather, resonances move to new positions, indicating that each peptide in a fibril interacts specifically with one or more NSAID molecules.

Upon addition of sulindac sulfide, CSPs are observed in particular for hydrophobic residues, such as, V18, F19 and F20, G33, M35, but also for the polar side chain of K16. The most dramatic CSPs are detected for K16 and G33 (Figure 1d).  $^{13}\text{C-}^{19}\text{F}$  REDOR experiments yield unambiguous distance restraints. The REDOR experiments show that sulindac sulfide binds in the vicinity of methyl groups of V18 or V39 as well as I31 and I32 C $\gamma$ 2.

In order to identify trends and avoid bias, we use both the 2-fold-symmetric (PDB-ID: 2LMN) (53), as well as the 3-fold-symmetric (PDB-ID: 2LMP) (54)  $A\beta_{1-40}$  fibrils as reference structures for modeling and docking experiments. The polymorphism of these structures may differ from the fibrils investigated in this study, however they show the highest similarities out of all three wild type  $A\beta_{1-40}$  fibril structures currently available (53,54,64). Within the two AB fibril structural ensembles, several hydrophobic cavities are detected which are large enough to potentially host a sulindac sulfide molecule. We did not find significant deviations in the distribution, size and polarity of the cavities in between the analyzed structural ensembles and models. Hence, changes in fibril polymorphism do not affect significantly the distribution of hydrophobic patches in amyloid fibrils. We conclude that the two employed structures provide a suitable basis for docking experiments, which are additionally supported by experimental NMR data, although high-resolution structures of a better defined polymorph will allow more accurate docking in the future.

An induced fit docking reveals that the NSAID can interact with fibrils in three different ways, whereby all models fulfill the NMR restraints. The apparently ambiguous REDOR restraints suggest that more than one sulindac sulfide molecule might be involved in binding. In the docking poses that are in best agreement with the NMR restraints, sulindac sulfide intercalates between the two  $\beta$ -strands of the A $\beta$  fibril, with the normal of the aromatic ring either parallel (Figure 4a/b, pose 1) or perpendicular (Figure 4a pose 2, Figure 4b poses 2 and 3) to the fibril axis. Thereby, residue F19 seems to play a crucial role in sulindac sulfide binding, as its rotameric state has an influence on the size and shape of cavities in clusters #2 and #3. Furthermore, the aromatic side chain is involved in  $\pi$ -stacking with the conjugated ring system of the NSAID.

Pose 1 of the docking approach suggests that sulindac sulfide fits into the groove formed by G33 (Figure 4a/b, top). Hence the large CSPs may be attributed to G33 backbone atoms experiencing a change in chemical environment, or even undergoing conformational changes to accommodate the NSAID. In theoretical studies, this glycine residue has been suggested to be

involved in oxidation of  $A\beta_{1-42}$ , due to its close proximity to the side-chain of M35 (73,74). Furthermore, G33 has been suggested as the key amino acid for  $A\beta$  toxicity, and is responsible for driving  $A\beta$  into neurotoxic conformations (75). Both residues, G33 and M35, have been hypothesized to stabilize reactive oxygen species (ROS) (76,77). Sulindac sulfide might therefore act by binding to the hydrophobic pocket in the vicinity of G33, thereby preventing oxidation of the  $A\beta$  peptide. Oxidation of  $A\beta_{1-42}$  reduces fibril assembly and aggregation, due to the increased polarity introduced by the methionine sulfoxide (78). In accordance, we find that the  $A\beta$ -sulindac sulfide complex exists in a stable fibrillar state.

CSPs for K16 may be explained by a recent docking study involving sulindac sulfide and A $\beta$  fibrils, which suggested that sulindac sulfide may bind weakly to a shallow, solvent-exposed pocket in the vicinity of K16 and V18, and does not interfere with fibrillation (30). This binding mode may in addition account for the large REDOR signal detected for the overlapping resonances V18/V39 C $\gamma$  (Figure 2a). We cannot exclude docking of sulindac sulfide to the fibril surface, as our REDOR and CSP data are also in agreement with the blind docking model proposed by Yesuvadian *et al* (30).

Sulindac sulfide has been reported to form colloidal aggregates above a critical micelle concentration (CMC) in solution (28). This commonly phenomenon is observed hydrophobic compounds (79,80). The size of small molecule colloidal particles is typically on the order of 50-600 nm (28). These colloids bind unfolded proteins in a promiscuous manner (79,80), and have been shown to lead to precipitation and inhibition of protein function (81-83). However, the effect of sulindac sulfide on Aß fibril chemical shifts reported here indicates not a promiscuous, but a specific interaction. Aggregates of the compound are observed in TEM images (Figure 1b), implying the presence of colloids in solution. This is expected, as the concentration used (250 µM) lies above the CMC of  $50\text{-}100\,\mu\text{M}$  (28). To account for the experimental single set of resonances, we must assume that individual NSAID molecules dissociate from the colloidal complexes, and interact specifically with A\beta fibrils.

Binding of sulindac sulfide in different cavities for different  $A\beta$  peptides would result in a splitting of the resonances and line broadening. We observe, however, narrow lines indicating that the small molecule must either bind simultaneously to different cavities or exchange between these cavities. Relaxation experiments will be carried out in the future to differentiate between these two scenarios.

In conclusion, we suggest that the NSAID sulindac sulfide is able to interact with Aß fibrils in a rather specific manner. We find that several cavities can accommodate a sulindac sulfide molecule. This is supported by defined CSPs and <sup>13</sup>C-<sup>19</sup>F REDOR contacts. Sulindac sulfide does not induce drastic architectural changes to the nontoxic fibrillar structure, as indicated by NMR and EM. In addition, the characteristic D23-K28 salt bridge, as well as length and positioning of the  $\beta$ strands is not affected. The molecular modeling analysis suggests that sulindac sulfide intercalates between the two  $\beta$ -strands at presumably more than one position. The presented data contributes to elucidating the mechanism by which small molecules bind insoluble amyloids. understanding is crucial for the design of pharmacologically relevant molecules, which interfere with AB species, and which might in the future be employed for the treatment of Alzheimer's disease.

#### ACKNOWLEDGMENTS

This work was performed in the framework of SFB-1035/Project-B07 (German Research Foundation, DFG). We acknowledge support by the Helmholtz-Gemeinschaft and the Deutsche Forschungsgemeinschaft (Grants Re1435). We are also grateful to the Center for Integrated Protein Science Munich (CIPS-M) for financial support. This work was also supported by grants from the Canadian Institute of Health Research grant (MOP-133411) and infrastructure awarded to G.M.. G.M. holds a Canada Research Chair in Molecular Pharmacology and CFI grants.

#### **CONFLICT OF INTEREST**

The authors declare no competing financial interest.

#### **AUTHOR CONTRIBUTION**

E.P. expressed and purified isotopically labelled peptide samples, designed and performed NMR experiments and carried out the data analysis. R.S. implemented solid-state NMR experiments. J.M.L.d.A recorded initial experiments and assisted with the data analysis. G.A-O. carried out the fluorine REDOR experiments. H.J.B. and P.W.H. performed and analyzed molecular modeling and docking. All authors discussed the results. B.R. and E.P. conceived the project and wrote the paper with input from all authors.

#### REFERENCES

- 1. Bucciantini, M., Giannoni, E., Chiti, F., Baroni, F., Formigli, L., Zurdo, J., Taddei, N., Ramponi, G., Dobson, C. M., and Stefani, M. (2002) Inherent toxicity of aggregates implies a common mechanism for protein misfolding diseases. *Nature* **416**, 507-511
- 2. Haass, C. (2004) Take five--BACE and the gamma-secretase quartet conduct Alzheimer's amyloid beta-peptide generation. *EMBO J.* **23**, 483-488
- 3. Kang, J., Lemaire, H. G., Unterbeck, A., Salbaum, J. M., Masters, C. L., Grzeschik, K. H., Multhaup, G., Beyreuther, K., and Muller-Hill, B. (1987) The precursor of Alzheimer's disease amyloid A4 protein resembles a cell-surface receptor. *Nature* 325, 733-736
- Olsson, F., Schmidt, S., Althoff, V., Munter, L. M., Jin, S., Rosqvist, S., Lendahl, U., Multhaup, G., and Lundkvist, J. (2014) Characterization of intermediate steps in amyloid beta (Abeta) production under near-native conditions. J. Biol. Chem. 289, 1540-1550
- 5. Roher, A. E., Lowenson, J. D., Clarke, S., Woods, A. S., Cotter, R. J., Gowing, E., and

- Ball, M. J. (1993) beta-Amyloid-(1-42) is a major component of cerebrovascular amyloid deposits: implications for the pathology of Alzheimer disease. *Proc. Natl. Acad. Sci. USA* **90**, 10836-10840
- 6. Prelli, F., Castano, E., Glenner, G. G., and Frangione, B. (1988) Differences between vascular and plaque core amyloid in Alzheimer's disease. *J Neurochem* **51**, 648-651
- 7. Selkoe, D. J. (2008) Soluble oligomers of the amyloid beta-protein impair synaptic plasticity and behavior. *Behav. Brain Res.* **192**, 106-113
- Bieschke, J., Russ, J., Friedrich, R. P., Ehrnhoefer, D. E., Wobst, H., Neugebauer, K., and Wanker, E. E. (2010) EGCG remodels mature alpha-synuclein and amyloid-beta fibrils and reduces cellular toxicity. *Proc. Natl. Acad. Sci. USA* 107, 7710-7715
- Bieschke, J., Herbst, M., Wiglenda, T., Friedrich, R. P., Boeddrich, A., Schiele, F., Kleckers, D., Lopez del Amo, J. M., Gruning, B. A., Wang, Q., Schmidt, M. R., Lurz, R., Anwyl, R., Schnoegl, S., Fandrich, M., Frank, R. F., Reif, B., Gunther, S., Walsh, D. M., and Wanker, E. E. (2012) Small-molecule conversion of toxic oligomers to nontoxic beta-sheet-rich amyloid fibrils. *Nat. Chem. Biol.* 8, 93-101
- 10. Akiyama, H., Barger, S., Barnum, S., Bradt, B., Bauer, J., Cole, G. M., Cooper, N. R., Eikelenboom, P., Emmerling, M., Fiebich, B. L., Finch, C. E., Frautschy, S., Griffin, W. S., Hampel, H., Hull, M., Landreth, G., Lue, L., Mrak, R., Mackenzie, I. R., McGeer, P. L., O'Banion, M. K., Pachter, J., Pasinetti, G., Plata-Salaman, C., Rogers, J., Rydel, R., Shen, Y., Streit, W., Strohmeyer, R., Tooyoma, I., Van Muiswinkel, F. L., Veerhuis, R., Walker, D., Webster, S., Wegrzyniak, B., Wenk, G., and Wyss-Coray, T. (2000) Inflammation and Alzheimer's disease. Neurobiol. Aging 21, 383-421
- 11. McGeer, P. L., and McGeer, E. G. (1995) The inflammatory response system of

- brain: implications for therapy of Alzheimer and other neurodegenerative diseases. *Brain Res. Brain Res. Rev.* **21**, 195-218
- 12. in t' Veld, B. A., Ruitenberg, A., Hofman, A., Launer, L. J., van Duijn, C. M., Stijnen, T., Breteler, M. M., and Stricker, B. H. (2001) Nonsteroidal antiinflammatory drugs and the risk of Alzheimer's disease. *N. Engl. J. Med.* **345**, 1515-1521
- Weggen, S., Eriksen, J. L., Sagi, S. A., Pietrzik, C. U., Ozols, V., Fauq, A., Golde, T. E., and Koo, E. H. (2003) Evidence that nonsteroidal anti-inflammatory drugs decrease amyloid beta 42 production by direct modulation of gamma-secretase activity. *J. Biol. Chem.* 278, 31831-31837
- 14. Eriksen, J. L., Sagi, S. A., Smith, T. E., Weggen, S., Das, P., McLendon, D. C., Ozols, V. V., Jessing, K. W., Zavitz, K. H., Koo, E. H., and Golde, T. E. (2003) NSAIDs and enantiomers of flurbiprofen target gamma-secretase and lower Abeta 42 in vivo. *J. Clin. Invest.* **112**, 440-449
- 15. Takahashi, Y., Hayashi, I., Tominari, Y., Rikimaru, K., Morohashi, Y., Kan, T., Natsugari, H., Fukuyama, T., Tomita, T., and Iwatsubo, T. (2003) Sulindac sulfide is a noncompetitive gamma-secretase inhibitor that preferentially reduces Abeta 42 generation. *J. Biol. Chem.* **278**, 18664-18670
- 16. Wanngren, J., Ottervald, J., Parpal, S., Portelius, E., Stromberg, K., Borgegard, T., Klintenberg, R., Jureus, A., Blomqvist, J., Blennow, K., Zetterberg, H., Lundkvist, J., Rosqvist, S., and Karlstrom, H. (2012) Second generation gamma-secretase modulators exhibit different modulation of Notch beta and Abeta production. *J. Biol. Chem.* 287, 32640-32650
- 17. Nadezhdin, K. D., Bocharova, O. V., Bocharov, E. V., and Arseniev, A. S. (2012) Dimeric structure of transmembrane domain of amyloid precursor protein in micellar environment. *FEBS Lett.* **586**, 1687-1692

- Chen, W., Gamache, E., Rosenman, D. J., Xie, J., Lopez, M. M., Li, Y. M., and Wang, C. (2014) Familial Alzheimer's mutations within APPTM increase Abeta42 production by enhancing accessibility of epsilon-cleavage site. *Nat. Commun.* 5, 3037
- 19. Barrett, P. J., Song, Y., Van Horn, W. D., Hustedt, E. J., Schafer, M., Hadziselimovic, A., Beel, A. J., and Sanders, C. R. (2012) The amyloid precursor protein has flexible а transmembrane domain binds and cholesterol. Science 336, 1168-1171
- 20. Manrique-Moreno, M., Garidel, P., Suwalsky, M., Howe, J., and Brandenburg, K. (2009) The membrane-activity of Ibuprofen, Diclofenac, and Naproxen: a physico-chemical study with lecithin phospholipids. *Biochim. Biophys. Acta* **1788**, 1296-1303
- Husch, J., Dutagaci, B., Glaubitz, C., Geppert, T., Schneider, G., Harms, M., Muller-Goymann, C. C., Fink, L., Schmidt, M. U., Setzer, C., Zirkel, J., Rebmann, H., Schubert-Zsilavecz, M., and Abdel-Tawab, M. (2011) Structural properties of so-called NSAID-phospholipid-complexes. *Eur. J. Pharm. Sci.* 44, 103-116
- 22. Lichtenberger, L. M., Zhou, Y., Jayaraman, V., Doyen, J. R., O'Neil, R. G., Dial, E. J., Volk, D. E., Gorenstein, D. G., Boggara, M. B., and Krishnamoorti, R. (2012) Insight membrane into NSAID-induced alterations, pathogenesis and therapeutics: characterization of interaction of **NSAIDs** with phosphatidylcholine. Biochim. Biophys. Acta **1821**, 994-1002
- 23. Kukar, T. L., Ladd, T. B., Bann, M. A., Fraering, P. C., Narlawar, R., Maharvi, G. M., Healy, B., Chapman, R., Welzel, A. T., Price, R. W., Moore, B., Rangachari, V., Cusack, B., Eriksen, J., Jansen-West, K., Verbeeck, C., Yager, D., Eckman, C., Ye, W., Sagi, S., Cottrell, B. A., Torpey, J., Rosenberry, T. L., Fauq, A., Wolfe, M. S., Schmidt, B., Walsh, D. M., Koo, E. H., and

- Golde, T. E. (2008) Substrate-targeting gamma-secretase modulators. *Nature* **453**, 925-929
- 24. Botev, A., Munter, L. M., Wenzel, R., Richter, L., Althoff, V., Ismer, J., Gerling, U., Weise, C., Koksch, B., Hildebrand, P. W., Bittl, R., and Multhaup, G. (2011) The amyloid precursor protein C-terminal fragment C100 occurs in monomeric and dimeric stable conformations and binds gamma-secretase modulators. *Biochemistry* **50**, 828-835
- 25. Richter, L., Munter, L. M., Ness, J., Hildebrand, P. W., Dasari, M., Unterreitmeier, S., Bulic, B., Beyermann, M., Gust, R., Reif, B., Weggen, S., Langosch, D., and Multhaup, G. (2010) Amyloid beta 42 peptide (Abeta42)-lowering compounds directly bind to Abeta and interfere with amyloid precursor protein (APP) transmembrane dimerization. *Proc. Natl. Acad. Sci. USA* 107, 14597-14602
- 26. Khalifa, N. B., Van Hees, J., Tasiaux, B., Huysseune, S., Smith, S. O., Constantinescu, S. N., Octave, J. N., and Kienlen-Campard, P. (2010) What is the role of amyloid precursor protein dimerization? *Cell Adh. Migr.* **4**, 268-272
- 27. Beel, A. J., Barrett, P., Schnier, P. D., Hitchcock, S. A., Bagal, D., Sanders, C. R., and Jordan, J. B. (2009) Nonspecificity of binding of gamma-secretase modulators to the amyloid precursor protein. *Biochemistry* **48**, 11837-11839
- 28. Barrett, P. J., Sanders, C. R., Kaufman, S. A., Michelsen, K., and Jordan, J. B. (2011) NSAID-based gamma-secretase modulators do not bind to the amyloid-beta polypeptide. *Biochemistry* **50**, 10328-10342
- 29. Hirohata, M., Ono, K., Naiki, H., and Yamada, M. (2005) Non-steroidal anti-inflammatory drugs have anti-amyloidogenic effects for Alzheimer's beta-amyloid fibrils in vitro. *Neuropharmacology* **49**, 1088-1099

- 30. Yesuvadian, R., Krishnamoorthy, J., Ramamoorthy, A., and Bhunia, A. (2014)
  Potent gamma-secretase inhibitors/modulators interact with amyloid-beta fibrils but do not inhibit fibrillation: a high-resolution NMR study. Biochem. Biophys. Res. Commun. 447, 590-595
- 31. Prade, E., Lopez del Amo, J.-M., and Reif, B. (2014) CHAPTER 27 NMR Studies of Small Molecules Interacting with Amyloidogenic Proteins. in Advances in Biological Solid-State NMR: Proteins and Membrane-Active Peptides, The Royal Society of Chemistry. pp 533-555
- 32. Choi, J. S., Braymer, J. J., Nanga, R. P., Ramamoorthy, A., and Lim, M. H. (2010)
  Design of small molecules that target metal-A{beta} species and regulate metal-induced A{beta} aggregation and neurotoxicity. *Proc. Natl. Acad. Sci. USA* 107, 21990-21995
- Rezaei-Ghaleh, N., Andreetto, E., Yan, L. M., Kapurniotu, A., and Zweckstetter, M. (2011) Interaction between amyloid beta peptide and an aggregation blocker peptide mimicking islet amyloid polypeptide. *PLoS One* 6, e20289
- 34. Yoo, S. I., Yang, M., Brender, J. R., Subramanian, V., Sun, K., Joo, N. E., Jeong, S. H., Ramamoorthy, A., and Kotov, N. A. (2011) Inhibition of amyloid peptide fibrillation by inorganic nanoparticles: functional similarities with proteins. *Angew. Chem. Int. Ed. Engl.* **50**, 5110-5115
- 35. Vivekanandan, S., Brender, J. R., Lee, S. Y., and Ramamoorthy, A. (2011) A partially folded structure of amyloid-beta(1-40) in an aqueous environment. *Biochem. Biophys. Res. Commun.* **411**, 312-316
- 36. Ramamoorthy, A., and Lim, M. H. (2013) Structural characterization and inhibition of toxic amyloid-beta oligomeric intermediates. *Biophys. J.* **105**, 287-288
- 37. Lopez del Amo, J. M., Fink, U., Dasari, M., Grelle, G., Wanker, E. E., Bieschke, J., and Reif, B. (2012) Structural properties of EGCG-induced, nontoxic Alzheimer's

- disease Abeta oligomers. *J. Mol. Biol.* **421**, 517-524
- 38. Masuda, Y., Fukuchi, M., Yatagawa, T., Tada, M., Takeda, K., Irie, K., Akagi, K., Monobe, Y., Imazawa, T., and Takegoshi, K. (2011) Solid-state NMR analysis of interaction sites of curcumin and 42-residue amyloid beta-protein fibrils. *Bioorg. Med. Chem.* **19**, 5967-5974
- 39. Mithu, V. S., Sarkar, B., Bhowmik, D., Das, A. K., Chandrakesan, M., Maiti, S., and Madhu, P. K. (2014) Curcumin alters the salt bridge-containing turn region in amyloid beta(1-42) aggregates. *J. Biol. Chem.* **289**, 11122-11131
- 40. Sato, M., Murakami, K., Uno, M., Nakagawa, Y., Katayama, S., Akagi, K., Masuda, Y., Takegoshi, K., and Irie, K. (2013) Site-specific inhibitory mechanism for amyloid beta42 aggregation by catechol-type flavonoids targeting the Lys residues. *J. Biol. Chem.* **288**, 23212-23224
- 41. Schutz, A. K., Soragni, A., Hornemann, S., Aguzzi, A., Ernst, M., Bockmann, A., and Meier, B. H. (2011) The amyloid-Congo red interface at atomic resolution. *Angew. Chem. Int. Ed. Engl.* **50**, 5956-5960
- 42. Dasari, M., Espargaro, A., Sabate, R., Lopez del Amo, J. M., Fink, U., Grelle, G., Bieschke, J., Ventura, S., and Reif, B. (2011) Bacterial inclusion bodies of Alzheimer's disease beta-amyloid peptides can be employed to study native-like aggregation intermediate states. *Chembiochem* 12, 407-423
- 43. Walsh, D. M., Thulin, E., Minogue, A. M., Gustavsson, N., Pang, E., Teplow, D. B., and Linse, S. (2009) A facile method for expression and purification of the Alzheimer's disease-associated amyloid beta-peptide. *FEBS J.* **276**, 1266-1281
- 44. Lopez del Amo, J. M., Schmidt, M., Fink, U., Dasari, M., Fandrich, M., and Reif, B. (2012) An asymmetric dimer as the basic subunit in Alzheimer's disease amyloid beta fibrils. *Angew. Chem. Int. Ed. Engl.* **51**, 6136-6139

- 45. Bloembergen, N. (1949) On the interaction of nuclear spins in a crystalline lattice. *Physica* **15**, 386-426
- Szeverenyi, N. M., Sullivan, M. J., and Maciel, G. E. (1982) Observation of spin exchange by two-dimensional fourier transform 13C cross polarization-magicangle spinning. J. Magn. Reson. 47, 462-475
- 47. Hing, A. W., Vega, S., and Schaefer, J. (1992) Transferred-echo double-resonance NMR. *J. Magn. Reson.* **96**, 205-209
- 48. Hing, A. W., Vega, S., and Schaefer, J. (1993) Measurement of Heteronuclear Dipolar Coupling by Transferred-Echo Double-Resonance NMR. *J. Magn. Reson.* **103**, 151-162
- 49. Castellani, F., van Rossum, B. J., Diehl, A., Rehbein, K., and Oschkinat, H. (2003) Determination of solid-state NMR structures of proteins by means of three-dimensional 15N-13C-13C dipolar correlation spectroscopy and chemical shift analysis. *Biochemistry* **42**, 11476-11483
- 50. Takegoshi, K., Nakamura, S., and Terao, T. (2001) 13C–1H dipolar-assisted rotational resonance in magic-angle spinning NMR. *Chem. Phys. Lett.* **344**, 631-637
- 51. Gullion, T., and Schaefer, J. (1989) Rotational-echo double-resonance NMR. J. Magn. Reson. **81**, 196-200
- 52. Jaroniec, C. P., Filip, C., and Griffin, R. G. (2002) 3D TEDOR NMR experiments for the simultaneous measurement of multiple carbon-nitrogen distances in uniformly (13)C,(15)N-labeled solids. *J. Am. Chem. Soc.* **124**, 10728-10742
- 53. Petkova, A. T., Yau, W. M., and Tycko, R. (2006) Experimental constraints on quaternary structure in Alzheimer's betaamyloid fibrils. *Biochemistry* **45**, 498-512
- 54. Paravastu, A. K., Leapman, R. D., Yau, W. M., and Tycko, R. (2008) Molecular structural basis for polymorphism in Alzheimer's beta-amyloid fibrils. *Proc. Natl. Acad. Sci. USA* **105**, 18349-18354

- 55. Goede, A., Preissner, R., and Frömmel, C. (1997) Voronoi cell: New method for allocation of space among atoms: Elimination of avoidable errors in calculation of atomic volume and density. *J. Comput. Chem.* **18**, 1113-1123
- Rother, K., Hildebrand, P. W., Goede, A., Gruening, B., and Preissner, R. (2009) Voronoia: analyzing packing in protein structures. *Nucleic Acids Res.* 37, D393-395
- 57. Tsai, J., and Gerstein, M. (2002) Calculations of protein volumes: sensitivity analysis and parameter database. *Bioinformatics* **18**, 985-995
- 58. Delaunay, B. N. (1934) Sur la sphère vide. *B. Acad. Sci. USSR* **7**, 793-800
- 59. Zhang, L., and Hermans, J. (1996) Hydrophilicity of cavities in proteins. *Proteins* **24**, 433-438
- 60. Sherman, W., Day, T., Jacobson, M. P., Friesner, R. A., and Farid, R. (2006) Novel procedure for modeling ligand/receptor induced fit effects. *J. Med. Chem.* **49**, 534-553
- 61. Sherman, W., Beard, H. S., and Farid, R. (2006) Use of an induced fit receptor structure in virtual screening. *Chem. Biol. Drug Des.* **67**, 83-84
- 62. Schrödinger Release 2014-1: Maestro, v., Schrödinger, LLC, New York, NY, 2014.
- 63. Friesner, R. A., Banks, J. L., Murphy, R. B., Halgren, T. A., Klicic, J. J., Mainz, D. T., Repasky, M. P., Knoll, E. H., Shelley, M., Perry, J. K., Shaw, D. E., Francis, P., and Shenkin, P. S. (2004) Glide: a new approach for rapid, accurate docking and scoring. 1. Method and assessment of docking accuracy. *J. Med. Chem.* 47, 1739-1749
- 64. Lu, J. X., Qiang, W., Yau, W. M., Schwieters, C. D., Meredith, S. C., and Tycko, R. (2013) Molecular structure of beta-amyloid fibrils in Alzheimer's disease brain tissue. *Cell* **154**, 1257-1268
- 65. Petkova, A. T., Leapman, R. D., Guo, Z., Yau, W. M., Mattson, M. P., and Tycko, R. (2005) Self-propagating, molecular-level

- polymorphism in Alzheimer's betaamyloid fibrils. *Science* **307**, 262-265
- 66. Niu, Z., Zhao, W., Zhang, Z., Xiao, F., Tang, X., and Yang, J. (2014) The molecular structure of Alzheimer beta-amyloid fibrils formed in the presence of phospholipid vesicles. *Angew. Chem. Int. Ed. Engl.* **53**, 9294-9297
- 67. Bertini, I., Gonnelli, L., Luchinat, C., Mao, J., and Nesi, A. (2011) A new structural model of Abeta40 fibrils. *J. Am. Chem. Soc.* **133**, 16013-16022
- Petkova, A. T., Ishii, Y., Balbach, J. J., Antzutkin, O. N., Leapman, R. D., Delaglio, F., and Tycko, R. (2002) A structural model for Alzheimer's beta -amyloid fibrils based on experimental constraints from solid state NMR. *Proc. Natl. Acad. Sci. USA* 99, 16742-16747
- 69. Shen, Y., Delaglio, F., Cornilescu, G., and Bax, A. (2009) TALOS+: a hybrid method for predicting protein backbone torsion angles from NMR chemical shifts. *J. Biomol. NMR* **44**, 213-223
- 70. Tycko, R. (2006) Molecular structure of amyloid fibrils: insights from solid-state NMR. *Q. Rev. Biophys.* **39**, 1-55
- 71. Chimon, S., Shaibat, M. A., Jones, C. R., Calero, D. C., Aizezi, B., and Ishii, Y. (2007) Evidence of fibril-like beta-sheet structures in a neurotoxic amyloid intermediate of Alzheimer's beta-amyloid. *Nat. Struct. Mol. Biol.* **14**, 1157-1164
- 72. Ahmed, M., Davis, J., Aucoin, D., Sato, T., Ahuja, S., Aimoto, S., Elliott, J. I., Van Nostrand, W. E., and Smith, S. O. (2010) Structural conversion of neurotoxic amyloid-beta(1-42) oligomers to fibrils. *Nat. Struct. Mol. Biol.* 17, 561-567
- 73. Rauk, A., Armstrong, D. A., and Fairlie, D. P. (2000) Is Oxidative Damage by β-Amyloid and Prion Peptides Mediated by Hydrogen Atom Transfer from Glycine α-Carbon to Methionine Sulfur within β-Sheets? J. Am. Chem. Soc. 122, 9761-9767
- 74. Rauk, A., and Armstrong, D. A. (2000) Influence of  $\beta$ -Sheet Structure on the Susceptibility of Proteins to Backbone

- Oxidative Damage: Preference for  $\alpha C$ -Centered Radical Formation at Glycine Residues of Antiparallel  $\beta$ -Sheets. *J. Am. Chem. Soc.* **122**, 4185-4192
- 75. Harmeier, A., Wozny, C., Rost, B. R., Munter, L. M., Hua, H., Georgiev, O., Beyermann, M., Hildebrand, P. W., Weise, C., Schaffner, W., Schmitz, D., and Multhaup, G. (2009) Role of amyloid-beta glycine 33 in oligomerization, toxicity, and neuronal plasticity. *J. Neurosci.* **29**, 7582-7590
- 76. Kanski, J., Varadarajan, S., Aksenova, M., and Butterfield, D. A. (2002) Role of glycine-33 and methionine-35 in Alzheimer's amyloid beta-peptide 1-42associated oxidative stress and neurotoxicity. Biochim. Biophys. Acta **1586**, 190-198
- 77. Brunelle, P., and Rauk, A. (2002) The radical model of Alzheimer's disease: specific recognition of Gly29 and Gly33 by Met35 in a beta-sheet model of Abeta: an ONIOM study. *J. Alzheimers Dis.* **4**, 283-289
- 78. Hou, L., Kang, I., Marchant, R. E., and Zagorski, M. G. (2002) Methionine 35 oxidation reduces fibril assembly of the amyloid abeta-(1-42) peptide of Alzheimer's disease. *J. Biol. Chem.* **277**, 40173-40176
- 79. McGovern, S. L., Caselli, E., Grigorieff, N., and Shoichet, B. K. (2002) A common mechanism underlying promiscuous inhibitors from virtual and high-throughput screening. *J. Med. Chem.* **45**, 1712-1722
- 80. Coan, K. E. D., and Shoichet, B. K. (2008) Stoichiometry and physical chemistry of promiscuous aggregate-based inhibitors. J. Am. Chem. Soc. 130, 9606-9612
- 81. Hagerman, A. E., and Butler, L. G. (1981) The specificity of proanthocyanidinprotein interactions. *J. Biol. Chem.* **256**, 4494-4497
- 82. Feng, B. Y., Toyama, B. H., Wille, H., Colby, D. W., Collins, S. R., May, B. C., Prusiner, S. B., Weissman, J., and Shoichet, B. K.

(2008) Small-molecule aggregates inhibit amyloid polymerization. *Nat. Chem. Biol.* **4**, 197-199

83. Ono, K., Li, L., Takamura, Y., Yoshiike, Y., Zhu, L., Han, F., Mao, X., Ikeda, T., Takasaki, J., Nishijo, H., Takashima, A., Teplow, D. B., Zagorski, M. G., and Yamada, M. (2012) Phenolic compounds prevent amyloid beta-protein oligomerization and synaptic dysfunction by site-specific binding. *J. Biol. Chem.* **287**, 14631-14643

#### **FOOTNOTES**

#### **ABBREVIATIONS**

Aβ, amyloid-β; APP, amyloid precursor protein; APP-TMS, amyloid precursor protein transmembrane sequence; CMC, critical micelle concentration; CP, cross polarization; CSP, chemical shift perturbation; DARR, dipolar assisted rotational resonance; GSM, y-secretase modulator; MAS, magic angle spinning; NSAID, non-steroidal anti-inflammatory drug: PDSD. proton-driven spin diffusion; REDOR, rotational echo double resonance; TALOS+, torsion angle likeliness obtained from shift and sequence similarities+; TEDOR, transferred echo double resonance; TEM, transmission electron microscopy; vdW, van der Waals.

#### FIGURE LEGENDS

**Figure 1. The influence of sulindac sulfide on Aβ.** (a) Chemical structures of the NSAIDs sulindac sulfide. (b) TEM images of 50 μM Aβ fibrils in the absence (bottom) and presence (top) of a 5-fold molar excess of sulindac sulfide. The fibrillar character is maintained, and deposits of sulindac sulfide can be observed (scale bar = 200 nm). (c) 2D  $^{13}$ C- $^{15}$ N TEDOR spectra of Aβ amyloid fibrils incubated in the presence of a 5-fold molar excess of sulindac sulfide and 1% DMSO (red) and Aβ fibrils incubated with 1% DMSO (black) as a control. Corresponding  $^{13}$ C- $^{13}$ C correlation spectra are shown in Figure S1. The obtained  $^{13}$ C line widths are in the order or

120-200 Hz (data not shown). Sequential assignments are obtained from 3D NCACX and NCOCX experiments. Arrows indicate residues, which experience large chemical shift changes. (d) CSPs induced by sulindac sulfide on the NMR chemical shifts of  $A\beta_{1-40}$  fibrils. Differences in chemical shifts ( $\Delta\delta$  (ppm)) were calculated for  $^{13}C$  and  $^{15}N$  resonances according to  $\Delta\delta_C = [(\delta C_{sul} - \delta C_{ref})^2]^{1/2}$  and  $\Delta\delta_N = [(2/5*(\delta N_{sul} - \delta N_{ref}))^2]^{1/2},$  respectively.

Figure 2. <sup>13</sup>C-<sup>19</sup>F REDOR and <sup>13</sup>C-<sup>15</sup>N **TEDOR NMR experiments**. (a) <sup>13</sup>C-<sup>19</sup>F REDOR NMR experiments recorded to observe dephasing of Aβ <sup>13</sup>C nuclei in close proximity to the <sup>19</sup>F atom of sulindac sulfide. Experiments were run with mixing times of 1.1 ms (not shown), 2.2 ms and 4.4 ms. A list of all <sup>13</sup>C-<sup>19</sup>F contacts observed is found in Table S1. Recoupled and reference spectra were subtracted to identify affected <sup>13</sup>C resonances (red). For reference, a 1D-13C experiment without <sup>19</sup>F recoupling including all aliphatic resonances is shown (gray). (b) Analysis of the salt bridge involving residues D23 and K28. <sup>13</sup>C-<sup>15</sup>N TEDOR spectra show cross peaks between K28-Nζ and D23-Cγ in presence (red) and absence of sulindac sulfide (black). A TEDOR mixing time of 15.72 ms is employed. 1D traces extracted at the  $N\zeta$  chemical shifts are superimposed with the 1D-13C reference spectra of the respective sample (gray).

Figure 3. Packing analysis of Aβ structures. (a) Distribution of internal cavities in 3-fold symmetric  $A\beta_{1-40}$  fibrils (PDB-ID: 2LMP, model 1) (54) and (b) 2-fold symmetric  $A\beta_{1-40}$  fibrils (PDB-ID: 2LMN, model 1) (53). The figure shows a cross section perpendicular to the fibril axis. Each cavity is depicted as a sphere. The radius of the sphere corresponds to the average distance from the cavity center to the AB vdW surface. Water containing, polar cavities are colored in blue, hydrophobic cavities in gray. The names of the cavity clusters #1 to #5 are surrounded by red boxes and their approximate position is indicated. The protein backbones are depicted as cartoons, with side chains drawn as lines. Residues, which are as close as < 6 Å to the <sup>19</sup>F-atom of sulindac sulfide are highlighted using sticks. Residues I32 and V36 which define cavity clusters are

represented in magenta. A30, L34 and V39 are drawn in green. F19 is colored red. Termini are marked with N or C.

Figure 4. Induced fit docking of sulindac sulfide to Aβ. (a) Induced fit docking of sulindac sulfide to the hydrophobic cavity cluster #3 of the 3-fold symmetric A $\beta_{1-40}$  fibril structure (PDB-ID: 2LMP, model 1, pose 1 and 2) (54) and (b) to the hydrophobic cavity cluster #2 and #3 of the 2-

fold symmetric  $A\beta_{1-40}$  structure (PDB-ID: 2LMN, model 1, for cluster #2: pose 1 and cluster #3: pose 2 and 3) (53). Sulindac sulfide is depicted as blue sticks, the protein backbones as cartoon. Residues within 6 Å to the <sup>19</sup>F-atom of sulindac sulfide are depicted as sticks in magenta for the cavity cluster defining residues I32 and V36, and in green for A30, L34 and V39. F19 and G33 are colored in red.

### **FIGURES**

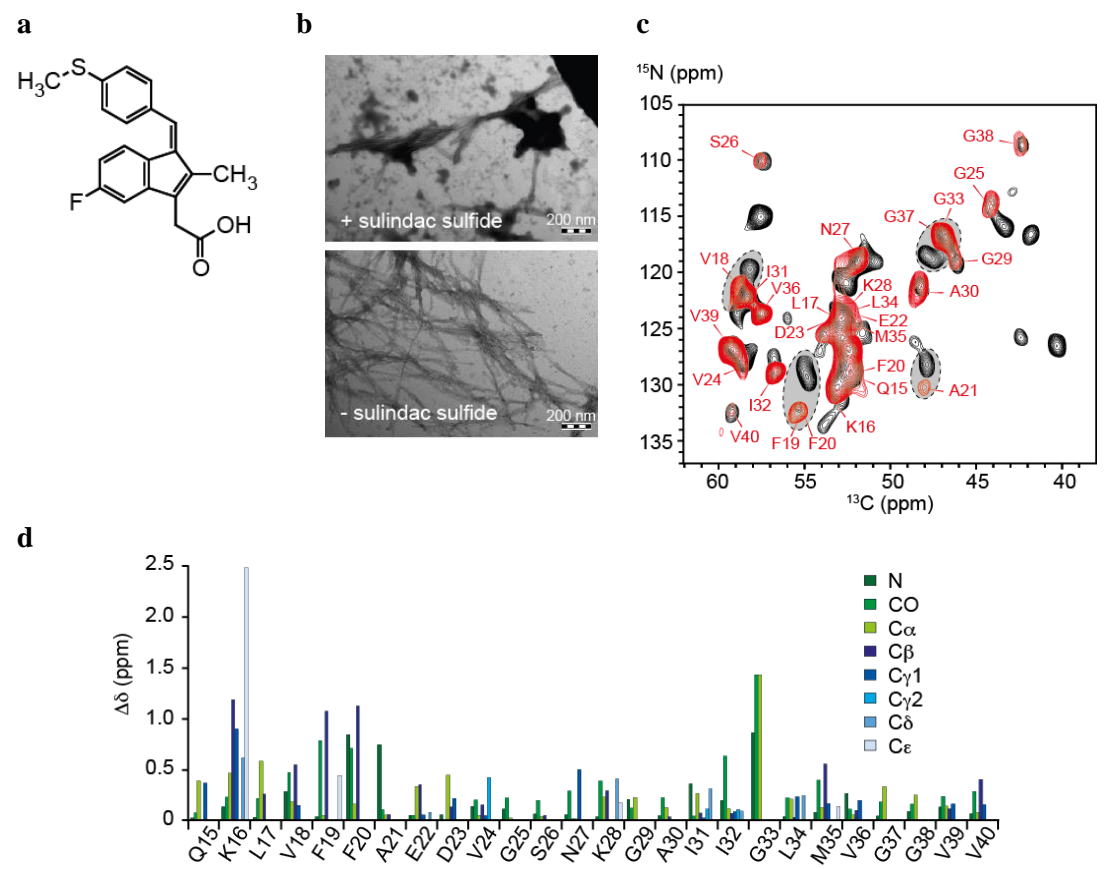


Figure 1. The influence of sulindac sulfide on Aβ.

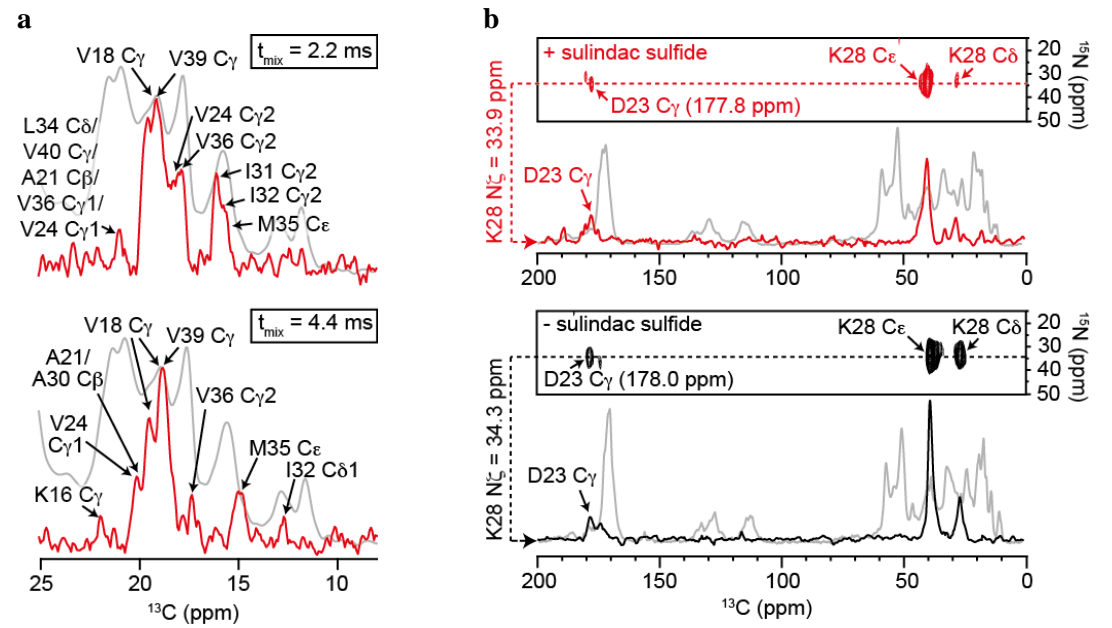


Figure 2. <sup>13</sup>C-<sup>19</sup>F REDOR and <sup>13</sup>C-<sup>15</sup>N TEDOR NMR experiments

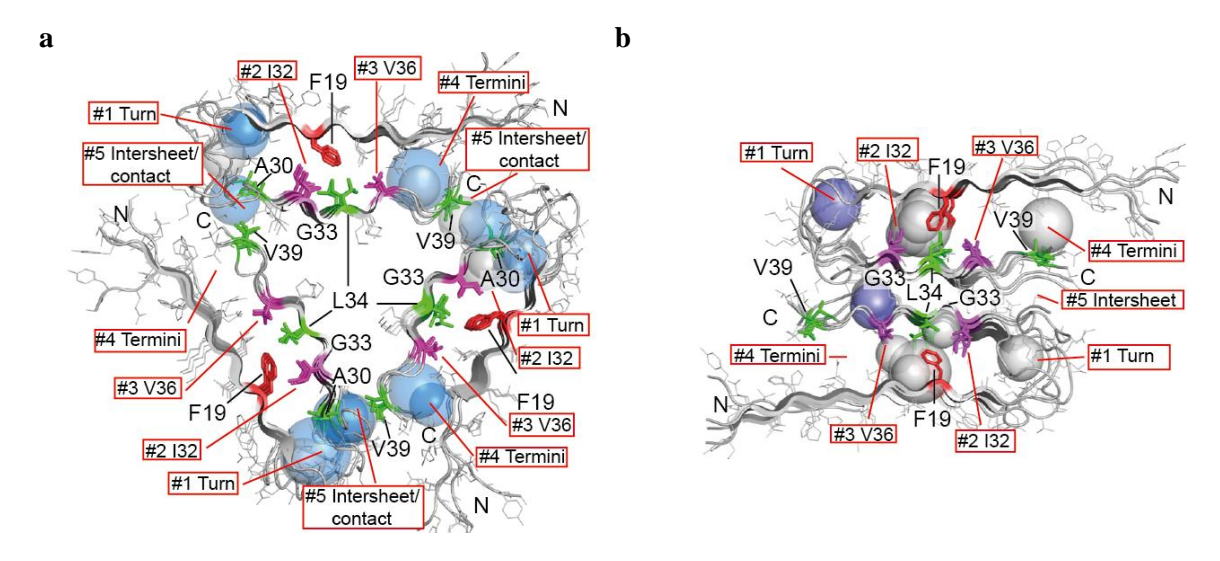


Figure 3. Packing analysis of  $A\beta$  structures.

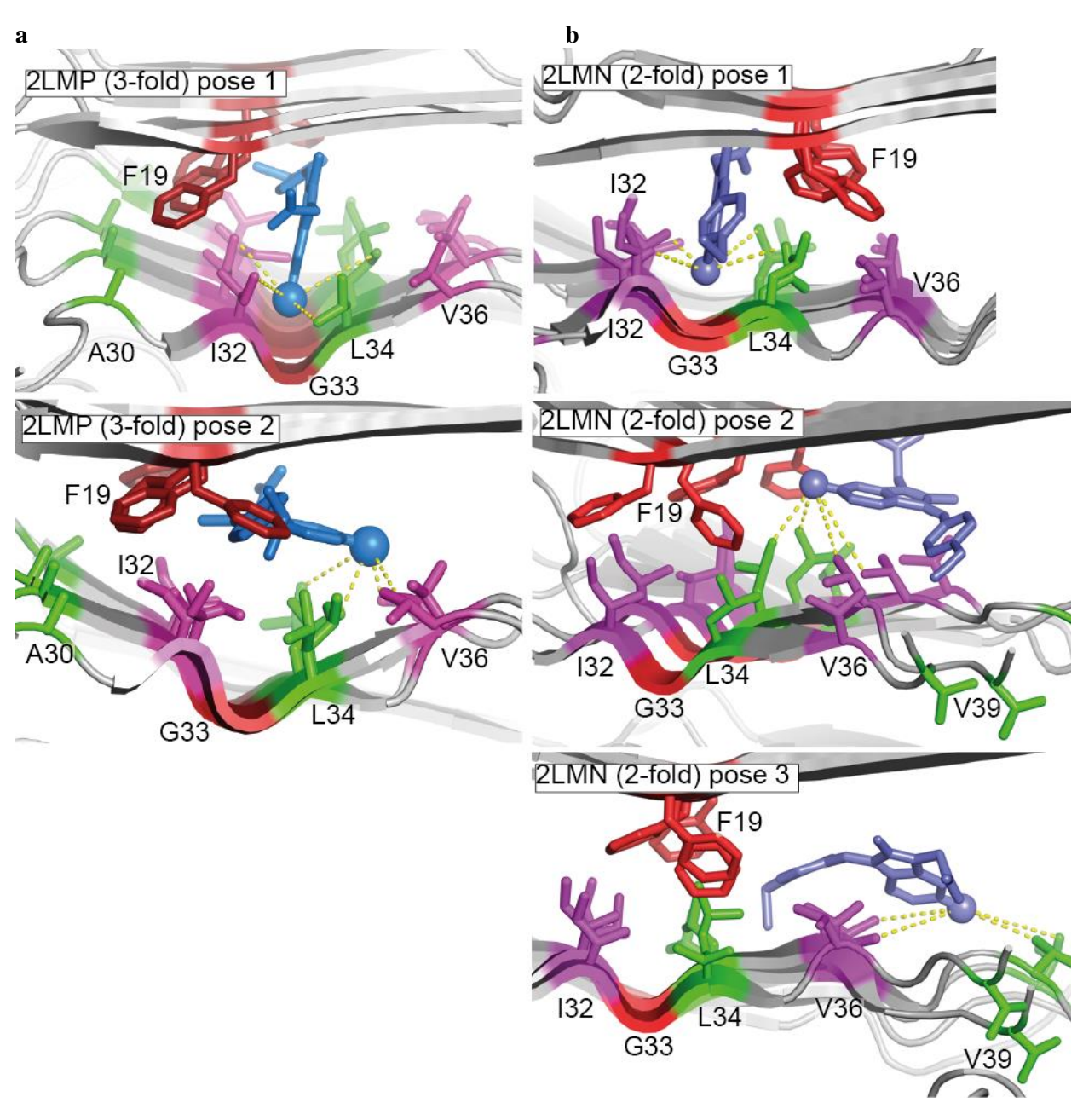


Figure 4. Induced fit docking of sulindac sulfide to  $A\beta$ .